MANSOURA JOURNAL OF PHYSICS
Official Journal of Faculty of Science, Mansoura University, Egypt
E-mail: scimag@mans.edu.eg ISSN: 2974-4954

The Effect of Cerium Oxide on the Structural Modifications of Hench Borate Bioglass and Glass-Ceramics

N. ElBaz[a], G. El-Damrawi[a], A. M. Abdelghany[b]*

[a] *Glass research group, Faculty of Science, Physics Department, Mansoura University, 35516, Mansoura, Egypt*

[b] *Spectroscopy Department, Physics Division, National Research Centre, 33 ElBehouth st., Dokki, 12311, Giza, Egypt*

Corresponding author: nadaelbaz94@yahoo.com

Received:21/6/2021
Accepted: 28/6/2021

Abstract: Glasses of modified Hench borate Bioglass containing gradient concentrations of cerium ions were prepared via an ordinary melting quenching route. Structural, mechanical, and morphological studies on the synthesized samples including X-ray diffraction (XRD), Scanning electron microscopic image supported with energy dispersive x-ray (SEM/EDAX), Fourier transforms infrared (FTIR) in combination with ^{31}P NMR spectroscopy were performed. It was noticed that samples containing less than 1 mol% CeO_2 are amorphous and their crystallinity increases with increasing Cerium content. The addition of more than 0.8 mol% CeO_2 can boost nucleation and crystallization processes, as well as the formation of various crystalline phases. Spectroscopic measurement in combination with deconvolution analysis technique (DAT) employed to calculate the number of tetrahedrally coordinated units of both boron and cerium atoms and therefore their structural role can be elevated.

Keywords: Cerium oxide; borate glass; FTIR; NMR; Vickers Hardness

1. Introduction

During the last decades, most research groups studied the formation and different applications of materials that contain the hydroxyapatite (HA) phase. HA is the mineral inorganic constituent of the human bones that assumed biocompatible with human hard tissues and shows osteoconductive properties [1-2]. Therefore, HA is considered a superior material with low mechanical characteristics compared with natural human bone. Bioactive glass-ceramics are being studied as fillers and bone graft alternatives to pure HA.

Unlike silicate glasses, without the creation of a borate-rich layer, bioactive borate glasses can generate hydroxyapatite right on the surface of the unreacted glass. This is because the borate matrix saturated with BO_3 groups, like phosphate glasses, is easily soluble in bodily fluids. Borate glasses can react to completion with no substantial change in dissolution kinetics because there is no diffusion layer [3, 4].

Previous research on bio-borate glasses has confirmed that the application based on bioactive borate glasses appears to be very useful, especially for bone growth and the efficacious healing of diabetic bone wounds [5-7]. Despite their excellent -bioactive properties, bioactive borate glasses have significant drawbacks, including low mechanical strength and fracture toughness. Because of this disadvantage, they can only be used in a few applications. In this thesis, we will conduct some scientific trials to improve mechanical performance while maintaining the benefit of good bioactivity. In this regard, rare earth oxides such as CeO_2 can be added to the glass matrix to convert the brittle bioactive glass into harder glass-ceramics containing some crystalline active phases. The following considerations must be carried out to satisfy the extremely good bioactivity and material strength:

The glass or glass-ceramics matrix should be prepared in such a way that it can contain

extremely variable concentrations of BO_3 units in both ring and non-ring configurations. . The bioactivity was previously known to be proportional to the glass's solubility, which is primarily determined by the BO_3 content [8, 9].

The cerium oxide should act as a glass former in the glass matrix, forming CeO_4 units at the expense of insoluble brittle BO_4 units. This means that in the glass network, CeO_4 tetrahedral units should be formed at the expense of BO_4 units only. The prepared sample's matrix must contain a crystalline cerium borate phase that is appropriate for strength achievement. Crystalline cerium calcium phosphate phases are also formed with care. At the beginning of crystal formation, the glass is suggested to be transparent. This results in a fine mixing of the various structural units that comprise the main glass network. . Furthermore, the size difference between amorphous and crystalline units should be very small [10-12].

Very advanced and powerful techniques, such as NMR spectroscopy of ^{11}B, Na, and ^{31}P resonances, should be used to guide us through the very limited changes that can be considered after CeO_2 addition. To recognize the effect of matrix on glass properties, the durability and hardness properties of some of the investigated samples should be reported [13].

Finally, the experimental results for both network extents of cerium-free and cerium-rich glasses should be reported. The preceding considerations may reflect our primary goal and objective from this study.

2. Materials and Techniques

Modified Hench Borate Bioglass consists of $x CeO_2.(45-x)B_2O_3.24.5Na_2O.24.5CaO.6P_2O_5$ were thermally synthesized through the melting process. Analytical grade cerium oxide provided by Sigma Company in combination with orthoboric acid, ammonium dihydrogen orthophosphate, sodium carbonate, and calcium carbonate supplied by Raysan Co. were used as sources for B_2O_3, P_2O_5, Na_2O, and CaO respectively. Samples composition were introduced in the table (1)

Precalculated amounts of chemicals were mixed and melted in porcelain crucibles at temperatures ranging between 1100-1200 °C depending on composition. The melts were then poured over a stainless-steel mold of required dimensions and allowed tope cooled gradually to room temperature. X-ray diffraction patterns were recorded via PANalytical X-Pert PRO operated at 30 Kv voltage adopting Cu target with wavelength k_α = 15.4 nm at Bragg's angles between 4 and 70°. Vickers's hardness numbers (H_V) was calculated as the average value of 10 indentations in triplicate samples via FM-7 microhardness tester with a fixed load of 25 g.

Table (1) sample name abbreviations and composition

Abbr.	CeO_2	B_2O_3	Na_2O	CaO	P_2O_5
Ce0	0.00	45.0	24.5	24.5	6.0
Ce0.5	0.50	44.5	24.5	24.5	6.0
Ce0.8	0.80	44.2	24.5	24.5	6.0
Ce1	1.00	44.0	24.5	24.5	6.0
Ce2	2.00	43.0	24.5	24.5	6.0
Ce4	4.00	41.0	24.5	24.5	6.0
Ce8	8.00	37.0	24.5	24.5	6.0
Ce12	12.0	33.0	24.5	24.5	6.0
Ce20	20.0	25.0	24.5	24.5	6.0

3. Results and Discussion

3.1. X-ray diffraction and Vickers microhardness

Figures 1 and 2 reveal the XRD pattern of both lower and higher contents of synthesized samples containing ceric oxide in different mass fractions. Samples that contain less than 0.8 CeO_2 (Figure 1) reveal a wide halo at about 25°, supporting the non-crystalline nature of prepared glasses, while other samples with a higher cerium oxide content up to 20 mole% (Figure 2) reveal intense sharp peaks superimposed over the non-crystalline diffraction halo indicating the formation of crystalline phase within the amorphous glassy matrix. The sharp intense peaks were compared with previously studied glasses with the nearly same composition and indexed to their respective phases [14]. Formed phases were compared to that of calcium cerium borate $Ca_2CeB_2O_7$ and sodium cerium borate $Na_4CeB_2O_7$, in combination with different calcium phosphates including $Ca_2(P_2O_7)$ and $CaCe(PO_3)$ which considered amongst the most bioactive and biocompatible glass phases [15-16].

The percent of crystallinity was determined from the area under associated crystalline peaks

(A_c) relative to that under both crystalline (A_c) and amorphous (A_a) bands in the XRD pattern, according to the following equation.

$$Cystallinity\ \% = \frac{A_c}{A_c + A_a} \times 100 \,. \qquad (1)$$

The percent of crystallinity is considered an indication for the bioactivity and tendency to form HA phase [17, 18]. Therefore, crystallinity considered sensitive to the variations in CeO_2 content as shown in Figure (3).

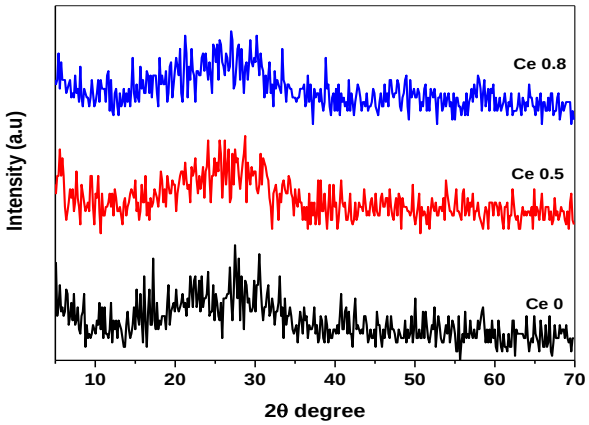

Fig. 1. XRD pattern of synthesized glass doped with up to 0.8 mol% Cerium oxide

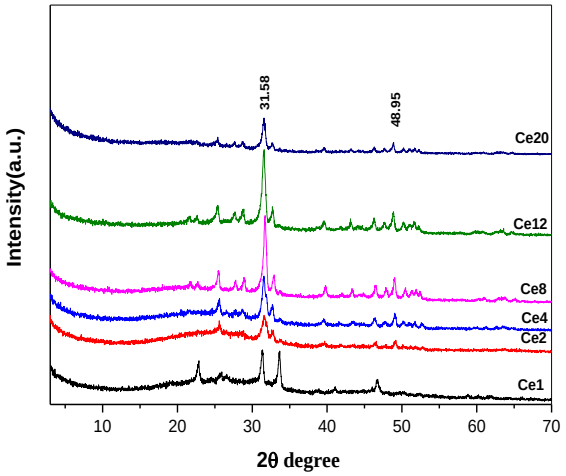

Fig. 2. XRD pattern of glasses containing Cerium oxide from 1 mol% up to 20 mol%

Table 2 crystallinity and Vickers microhardness number with CeO_2 content

Ce_2O (mol%)	20	12	8.0	4.0	2.0	1.0	0.8	0.5	0.0
Crystallinity%	65	70	65	43	25	17	0.0	0.0	0.0
H_v (kg/mm^2)	400	400	400	422	460	500	520	530	522

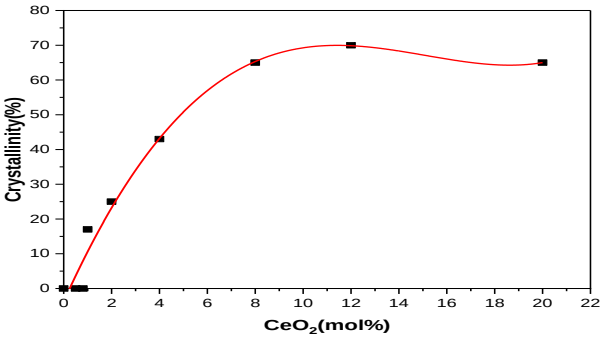

Fig. 3. crystallinity index of the studied glasses

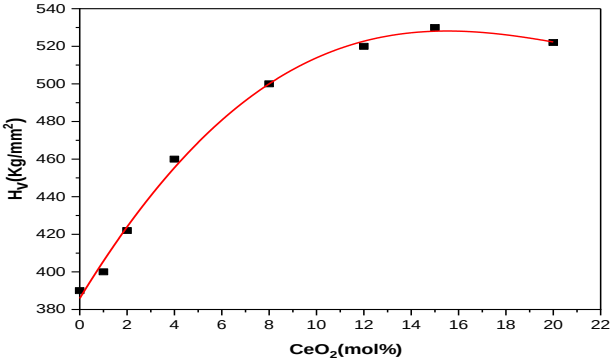

Fig. 4. Vickers's Hardness number as a function of cerium content

The percent crystallinity was found to be correlated to the hardness number of the studied samples and behaves nearly the same behavior. Calculated crystallinity % and Vickers microhardness number in correlation to cerium content were shown in Figures 3 & 4, and listed in table 2.

3.2. Scanning Electron Microscopy supported Energy Dispersive X-ray (SEM/EDAX)

Figure 4 reveals scanning electron micrograph images (SEM) that represent the topographic nature of the surface of two selected samples in the lower and higher cerium concentration regions. Significant differences in the topography of the studied samples with low CeO_2 (0.8 mol %) and with the higher CeO_2 content (20 mol %) were observed. It was clear that change in the cerium content results in the appearance of large crystalline species within the amorphous matrix as supported by XRD results. EDAX peaks were also interpreted in terms of cerium transitions within the molecular states of Lα and Mα originally located at about 4.8403 and 0.8831 keV respectively in combination with other transitions of constituting glass partners including Ca Lα, Ca Kα, Na Kα, O Kα and P

Kα at about 0.3413, 3.6905, 1.041, 0.5249 and 2.0134 keV respectively shown in Figures 5a, b [19].

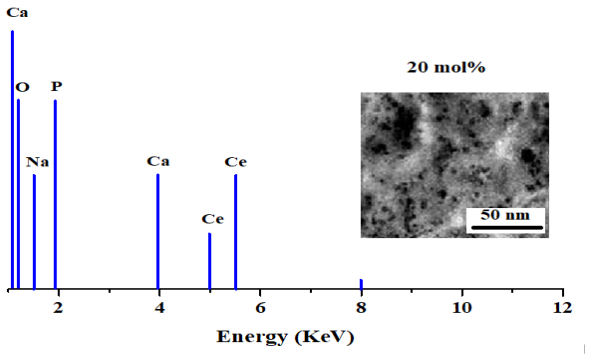

(a)

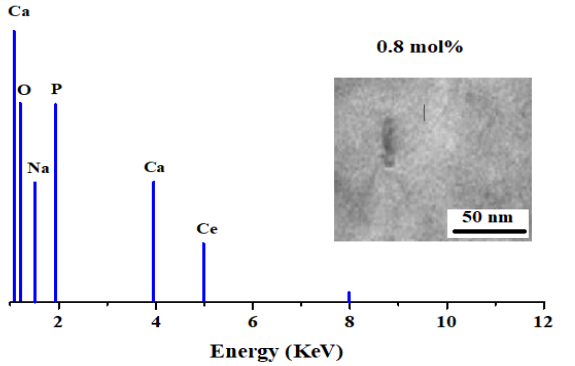

(b)

Fig. 5. SEM/EDAX images of extreme samples (a) 0.8 mol% and (b) 20 mol% CeO_2.

3.3. NMR and FTIR Correlation

NMR experiments offer direct information about the Q^n units in the glassy matrices containing multi-former oxide or intermediate partner with four coordinated oxygen. It is shown in Figure (6) that the chemical shift value of glasses with lower cerium oxide content up to 2 mol% (9 ppm) as a dominant structural species corresponding to orthophosphate units while the addition of cerium oxide changes the values of the chemical shift to about (2ppm) in the higher concentrations up to 20 mol% CeO_2 interpreted in terms of the interaction between cerium cation that coordinated with PO_4 groups forming a new cerium phosphate crystalline phases.

It was concluded that CeO_2 addition may be consumed in the phosphate and borate network modification causing an observed reduction in the number of four coordinated units (B_4) [20].

$$B_4 = \frac{BO_4 + CeO_4}{BO_4 + CeO_4 + BO_3} \qquad (2)$$

Such fact can be combined with the number of tetrahedral borate units that can be calculated from the deconvolution analysis technique (DAT) previously reported by different authors. Deconvoluted technique applied for both NMR and FTIR spectral data to calculate both B4 and N4. Figure (7) reveals FTIR optical absorption data of studied borate glasses containing different amounts of CeO_2 concentrations. While Figure (8) shows an exemplified analyzed sample in both techniques.

$$N_4 = \frac{BO_4}{BO_4 + BO_3} \qquad (3)$$

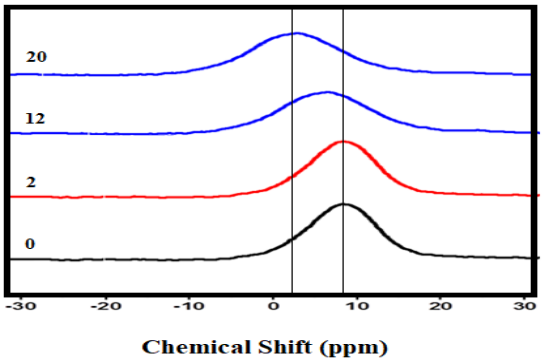

Fig. 6. NMR spectra of selected samples containing different CeO_2 concentrations

The concentration or fraction of CeO_2 as former CeO_4 units can be estimated from the difference between these two values (B4-N4) [21]

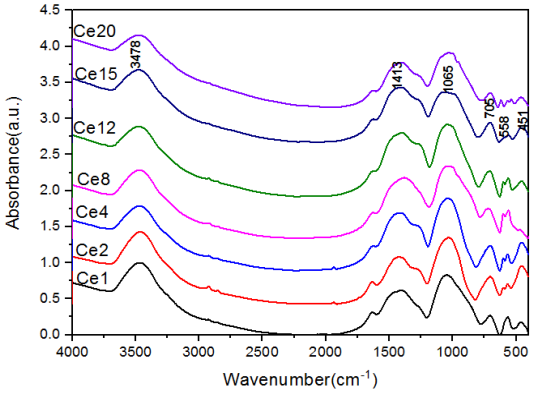

Fig. 7. FTIR absorption spectra of the studied samples

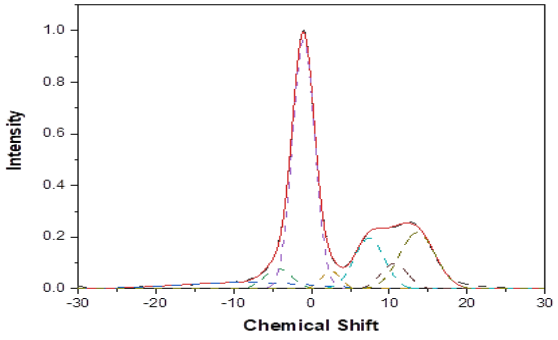

(a)

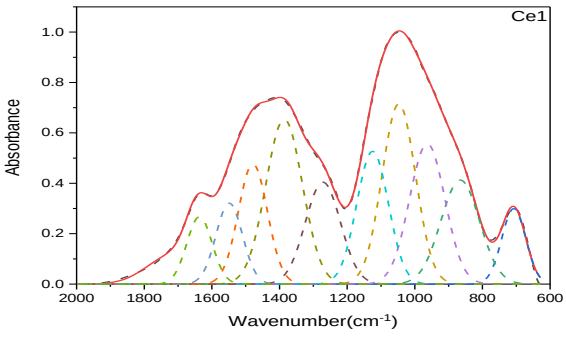

Fig. 8. deconvoluted spectra of selected sample containing 1 mol% CeO_2 (a) NMR and (b) FTIR

Figure (9) below shows the obtained values of both N_4 drawn from the FTIR spectral data analysis with the B_4 values obtained from the NMR spectral data analysis. It was clear that B_4 values are usually greater than that of N_4 except for the sample free of cerium oxide and generally constituting only BO_4 and BO_3 structural units. Samples containing cerium oxide as a former partner usually contain tetrahedral cerium structural units CeO_4 that cannot be separated or measured using the NMR analysis route. Therefore, the difference between these values introduces a suggested measure for these units and specifies the role of cerium in the structure.

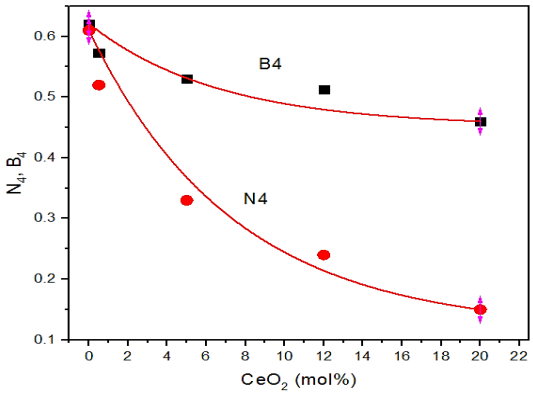

Fig. 9. Variation of N4 and B4 with the change of the cerium oxide content in the samples

4. Conclusions

Modified Hench Borate Bioglass containing variable amounts of cerium oxide up to 20 mol% were thermally synthesized through melting process. XRD data reveals formation of amorphous glasses containing up to 0.8 mol% cerium while samples containing higher concentration of cerium shows formation of crystalline phases attributed to the presence of cerium oxide as nucleating and crystallizing agent. The percent crystallinity also calculated from XRD data and their logarithmic behavior was discussed and correlated with the Vickers microhardness number. SEM/EDAX approves the presence of cerium ions as a glass former within the glassy matrix. FTIR/NMR spectroscopic data were used to calculate the fraction of tetra-coordinated units adopting DAT technique.

References

1. Han, Y., Wei, Q., Chang, P., Hu, K., Okoro, O. V., Shavandi, A., & Nie, L. (2021). Three-Dimensional Printing of Hydroxyapatite Composites for Biomedical Application. Crystals, **11(4),** 353.
2. Wu, Y., Hench, L. L., Du, J., Choy, K. L., & Guo, J. (2004). Preparation of hydroxyapatite fibers by electrospinning technique. *Journal of the American Ceramic Society*, **87(10),** 1988-1991.
3. Okasha, A., Abdelghany, A. M., Wassel, A. R., & Menazea, A. A. (2020). Bone bonding augmentation and synergetic attitude of gamma-irradiated modified borate bioglass. Radiation Physics and Chemistry, **176**, 109018.
4. Abdelghany, A. M., (2013). Novel method for early investigation of bioactivity in different borate bio-glasses. Spectrochimica Acta Part A: Molecular and Biomolecular Spectroscopy, **100,** 120-126.
5. Rahaman, M. N., Day, D. E., Bal, B. S., Fu, Q., Jung, S. B., Bonewald, L. F., & Tomsia, A. P. (2011). Bioactive glass in tissue engineering. Acta biomaterialia, **7(6),** 2355-2373.
6. Yao, A., Wang, D., Huang, W., Fu, Q., Rahaman, M. N., & Day, D. E. (2007). In vitro bioactive characteristics of borate-based glasses with controllable degradation behavior. *Journal of the American Ceramic Society*, ***90*(1),** 303-306.
7. Hench, L. L. (2006). The story of Bioglass®. *Journal of Materials Science: Materials in Medicine*, ***17*(11),** 967-978.
8. Yu, Y., & Edén, M. (2016). Structure–composition relationships of bioactive borophosphosilicate glasses probed by multinuclear 11 B, 29 Si, and 31 P solid

state NMR. RSC Advances, ***6*(103),** 101288-101303.

9. ElBatal, F. H., Abdelghany, A. M., ElDin, F. E., & ElBatal, H. A. (2020). Vanadium structural role in binary fluoride borate glasses and effects of gamma irradiation. Radiation Physics and Chemistry, **170**, 108659.
10. El-Damrawi, G., & El-Egili, K. (2001). Characterization of novel CeO_2–B_2O_3 glasses, structure and properties. Physica B: Condensed Matter, **299(1-2),** 180-186.
11. El-Damrawi, G., Gharghar, F., & Ramadan, R. M. (2016). Structural studies on new $xCeO_2 \cdot (50- x)\ PbO \cdot\ 50B_2O_3$ glasses and glass ceramics. *Journal of Non-Crystalline Solids*, **452**, 291-296.
12. Gjam, F. Z., Eldamrawi, G., Meikhail, M. S., & Abdelghany, M. (2021). Improving structure and properties of lead phosphate glass through precipitation of few crystals from CeO_2. *Egyptian Journal of Chemistry*.
13. Pedone, A., Charpentier, T., Malavasi, G., & Menziani, M. C. (2010). New insights into the atomic structure of 45S5 bioglass by means of solid-state NMR spectroscopy and accurate first-principles simulations. Chemistry of Materials, ***22*(19),** 5644-5652.
14. Lingtong, K. O. N. G., Hua, H. U., Tianyou, W. A. N. G., Huang, D., & Jianjian, F. U. (2011). Synthesis and surface modification of the nanoscale cerium borate as lubricant additive. *Journal of Rare Earths*, **29(11),** 1095-1099.
15. Barbi, S., Mugoni, C., Montorsi, M., Affatigato, M., Gatto, C., & Siligardi, C. (2018). Structural and optical properties of cerium oxide doped barium bismuth borate glasses. *Journal of Non-Crystalline Solids*, **499,** 183-188.
16. Muralimanohar, P., Parasuraman, R., Gandhi, J. R., Rathnakumari, M., & Sureshkumar, P. (2016). Photo-luminescence in cerium doped barium aluminium borate difluoride—$BaAlBO_3F_2$ glass ceramics. Optik, **127(20),** 8956-8962.
17. Li, B., Wang, S., & Fang, Y. (2017). Effect of Cr_2O_3 addition on crystallization, microstructure and properties of Li_2O–Al_2O_3–SiO_2 glass-ceramics. *Journal of Alloys and Compounds*, **693**, 9-15.
18. Doumeng, M., Makhlouf, L., Berthet, F., Marsan, O., Delbé, K., Denape, J., & Chabert, F. (2021). A comparative study of the crystallinity of polyetheretherketone by using density, DSC, XRD, and Raman spectroscopy techniques. Polymer Testing, **93,** 106878.
19. El-Damrawi, G., Abdelghany, A. M., Hassan, A. K., & Faroun, B. (2021). Effect of BO4 and FeO4 Structural Units on Conduction Mechanism of Iron Borosilicate Glasses. Silicon, 1-7. DOI-https://doi.org/10.1007/s12633-020-00694-w
20. ElBaz, N., El-Damrawi, G., & Abdelghany, A. M. (2021). Structural Role of CeO_2 in the Modified Borate Glass-Ceramics. *New Journal of Glass and Ceramics*, **11(1),** 34-43.
21. El-Damrawi, G., Abdelghany, A. M., Hassan, A. K., & Faroun, B. (2020). Conductivity and morphological studies on iron borosilicate glasses. *Journal of Non-Crystalline Solids*, **545,** 120233.